Vorticity in heavy-ion collisions at the JINR Nuclotron-based Ion Collider fAcility

Yu. B. Ivanov[1,2,*] and A. A. Soldatov[2,†]
[1]*National Research Centre "Kurchatov Institute", Moscow 123182, Russia*
[2]*National Research Nuclear University "MEPhI" (Moscow Engineering Physics Institute), Moscow 115409, Russia*
(Received 10 January 2017; published 31 May 2017)

Vorticity of matter generated in noncentral heavy-ion collisions at energies of the Nuclotron-based Ion Collider fAcility (NICA) at the Joint Institute for Nuclear Research (JINR) in Dubna is studied. Simulations are performed within the model of the three-fluid dynamics (3FD) which reproduces the major part of bulk observables at these energies. Comparison with earlier calculations is done. The qualitative pattern of the vorticity evolution is analyzed. It is demonstrated that the vorticity is mainly located at the border between participants and spectators. In particular, this implies that the relative Λ-hyperon polarization should be stronger at rapidities of the fragmentation regions than that in the midrapidity region.

DOI: 10.1103/PhysRevC.95.054915

I. INTRODUCTION

In peripheral collisions of high-energy heavy ions the system has a large angular momentum [1] that may result in observable consequences. The large angular momentum can manifest itself in a chiral vortical effect that results in induced currents and charge separation [2,3] similarly to the so-called chiral magnetic effect [4–6]. Another possible manifestation is the polarization of secondary produced particles [1,7–10]. Preliminary experimental results on hyperon polarization in heavy-ion collisions at energies of the Beam Energy Scan (BES) program at the Relativistic Heavy Ion Collider (RHIC) at Brookhaven were recently reported [11]. Experimental observation of these effects may give us additional information on the dynamics of heavy-ion collisions, e.g., on possible Kelvin-Helmholtz instability [12,13] or other turbulent phenomena [14].

The vorticity developed in heavy-ion collisions was estimated within various models. These estimates mainly concern the energies available at the Large Hadron Collider (LHC) and RHIC energies [15–19]. A comprehensive study of Λ polarization at BES-RHIC energies was recently done in Ref. [9]; it only partially overlapped with the NICA energy range. Only two recent studies [20,21] were dedicated to the lower energies of NICA at JINR. However, those studies [20,21] were performed within different approaches ([20] within the particle-in-cell relativistic (PICR) hydro approach [16] and [21] within the hadron-string dynamics model [22]) and for nuclear collisions at different collision energies, which makes their direct comparison difficult. Very recently the approach of Ref. [16] was further developed to estimate the Λ polarization at the top NICA energies [10].

In the present paper the vorticity is simulated within the 3FD model [23] for several collision energies in the NICA energy range. This study is also relevant to the recently announced STAR Fixed-Target Program at RHIC [24]. The 3FD model is quite successful in reproduction of the major part of bulk observables: the baryon stopping [25,26], yields of different hadrons, their rapidity and transverse momentum distributions [27,28], and the elliptic [29] and directed [30] flow excitation functions. Therefore, it would be instructive to compare the 3FD vorticity pattern with those in the above mentioned approaches [20,21].

II. VORTICITY IN THE 3FD MODEL

There are several definitions of the vorticity used in the literature that are suitable for analyzing different aspects of the rotation effects. In the present study we consider two of them. The first one is the relativistic kinematic vorticity

$$\omega_{\mu\nu} = \tfrac{1}{2}(\partial_\nu u_\mu - \partial_\mu u_\nu), \tag{1}$$

where u_μ is a collective local four-velocity of the matter. This type of the vorticity is directly relevant to the chiral vortical effect [3] that is caused by coupling to medium vorticity and leads to a contribution to the electromagnetic current

$$J^\kappa_{\rm e} = \frac{N_c}{4\pi^2 N_f}\varepsilon^{\kappa\lambda\mu\nu}\partial_\mu u_\nu\,\partial_\lambda\left(\theta\sum_j e_j\mu_j\right), \tag{2}$$

where N_c and N_f are the number of colors and flavors respectively, e_j and μ_j are the electric charge and chemical potential of a particle of j flavor, respectively, and θ is the topological QCD field.

Another type of the vorticity is so-called thermal vorticity,

$$\varpi_{\mu\nu} = \tfrac{1}{2}(\partial_\nu\hat\beta_\mu - \partial_\mu\hat\beta_\nu), \tag{3}$$

where $\hat\beta_\mu = \hbar\beta_\mu$ and $\beta_\mu = u_\nu/T$, with T being the local temperature. Thus, ϖ is dimensionless. It is directly related to the polarization vector, $\Pi^\mu(p)$, of a spin 1/2 particle in a relativistic fluid [31],

$$\Pi^\mu(p) = \frac{1}{8m}\frac{\int_\Sigma {\rm d}\Sigma_\lambda p^\lambda n_F(1-n_F)\,p_\sigma\epsilon^{\mu\nu\rho\sigma}\partial_\nu\beta_\rho}{\int_\Sigma \Sigma_\lambda p^\lambda\, n_F}, \tag{4}$$

where n_F is the Fermi-Dirac-Juttner distribution function and the integration runs over the freeze-out hypersurface Σ.

Unlike the conventional hydrodynamics, where local instantaneous stopping of projectile and target matter is assumed,

*y.ivanov@gsi.de
†saa@ru.net

a specific feature of the 3FD description [23] is a finite stopping power resulting in a counterstreaming regime of leading baryon-rich matter. This generally nonequilibrium regime of the baryon-rich matter is modeled by two interpenetrating baryon-rich fluids initially associated with constituent nucleons of the projectile (p) and target (t) nuclei. In addition, newly produced particles, populating the midrapidity region, are associated with a fireball (f) fluid. At later stages the baryon-rich and fireball fluids may consist of any type of hadrons and/or partons (quarks and gluons), rather than only nucleons and pions. Each of these fluids is governed by conventional hydrodynamic equations coupled by friction terms in the right-hand sides of the Euler equations. These friction terms describe energy-momentum loss of the baryon-rich fluids.

Thus, the system is characterized by three hydrodynamical velocities, u^μ_α with $\alpha =$ p, t and f, attributed to these fluids. At NICA energies the interpenetration of the p and t fluids takes place only at the initial stage of the nuclear collision. At later stages a complete mutual stopping occurs and these fluids get unified. Therefore, we define a collective four-velocity of the baryon-rich matter associating it with the total baryon current,

$$u^\mu_B = J^\mu_B/|J_B|, \tag{5}$$

where $J^\mu_B = n_p u^\mu_p + n_t u^\mu_t$ is the baryon current defined in terms of proper baryon densities n_α and hydrodynamic four-velocities u^μ_α, and

$$|J_B| = \left(J^\mu_B J_{B\mu}\right)^{1/2} \equiv n_B \tag{6}$$

is the proper (i.e., in the local rest frame) baryon density of the p and t fluids. In particular, this proper baryon density allows us to construct a simple fluid unification measure

$$1 - \frac{n_p + n_p}{n_B} \tag{7}$$

which is zero, when the p and t fluids are mutually stopped and unified, and has a positive value increasing with rise of the relative velocity of the p and t fluids.

The energy accumulated by the fireball fluid is an order of magnitude lower than that in the baryon-rich fluids even at $\sqrt{s_{NN}} = 9.2$ GeV, i.e. the top NICA energy. Therefore, we concentrate on the vorticity of the baryon-rich fluids. Thus, the vorticities of Eqs. (1) and (3) are considered in terms of u^μ_B.

The temperature, T_B, that is required in calculations of the thermal vorticity (3), also needs some comments. It is defined as a local proper-energy-density-weighted temperature

$$T_B = \sum_{\alpha=\mathrm{p,t}} T_\alpha \varepsilon_\alpha \Big/ \sum_{\alpha=\mathrm{p,t}} \varepsilon_\alpha, \tag{8}$$

where ε_α is the proper energy density of the α fluid. At the initial nonequilibrium stage of the collision (i.e., at $t \lesssim 4$ fm/c for 4.9 GeV and $t \lesssim 2$ fm/c for 7.7 GeV for midcentral Au+Au collisions considered below) this quantity does not relate to a true temperature of the system just because the temperature concept is inapplicable to a strongly nonequilibrium system. However, this temperature is close to the true temperature of the system at the expansion stage of the collision, when baryon-rich fluids are practically unified.

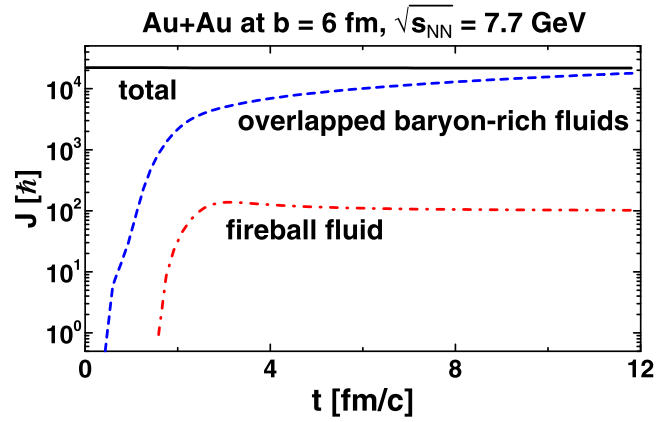

FIG. 1. Time evolution of the total angular momentum (conserved quantity), the angular momentum of the baryon-rich fluids in their overlap region, and the angular momentum of the fireball fluid in the semicentral ($b = 6$ fm) Au+Au collision at $\sqrt{s_{NN}} =$ 7.7 GeV. Calculations are done with the crossover EoS.

The physical input of the present 3FD calculations is described in Ref. [25]. The friction between fluids was fitted to reproduce the stopping power observed in proton rapidity distributions for each EoS, as described in Ref. [25] in detail. The simulations in [25–30] were performed with different equations of state (EoS's): a purely hadronic EoS [32] and two versions of the EoS involving the deconfinement transition [33], i.e., a first-order phase transition and a smooth crossover one. In the present paper we demonstrate results with only the crossover EoS as the most successful in reproduction of various bulk observables.

In Fig. 1 the time evolution of the total angular momentum, the angular momentum of the baryon-rich fluids in their overlap region, and the angular momentum of the fireball fluid in the semicentral ($b = 6$ fm) Au+Au collision at $\sqrt{s_{NN}} =$ 7.7 GeV are presented. The total angular momentum (that includes a contribution of spectators) is a conserved quantity. Therefore, its constancy demonstrates the accuracy of the numeric scheme: J_{total} is conserved with the accuracy of 1.5%. The overlap region rises in the course of interpenetration of nuclei and then at the expansion stage this region includes more and more former spectators. Thus, the angular momentum of the baryon-rich fluids in their overlap almost completely involves the total angular momentum of the system at the final stage of the collision. The angular momentum of the newly produced f fluid is almost two orders of magnitude lower than that of the overlapped baryon-rich fluids at the considered collision energy. Moreover, the baryon-rich fluids and fireball fluid are located in the same rapidity range at the considered collision energy. These are additional arguments to neglect the contribution of the fireball fluid vorticity in the consideration below.

III. RESULTS

The 3FD simulations of Au+Au collisions were performed without freeze-out. The freeze-out in the 3FD model removes the frozen out matter from the hydrodynamical evolution [34].

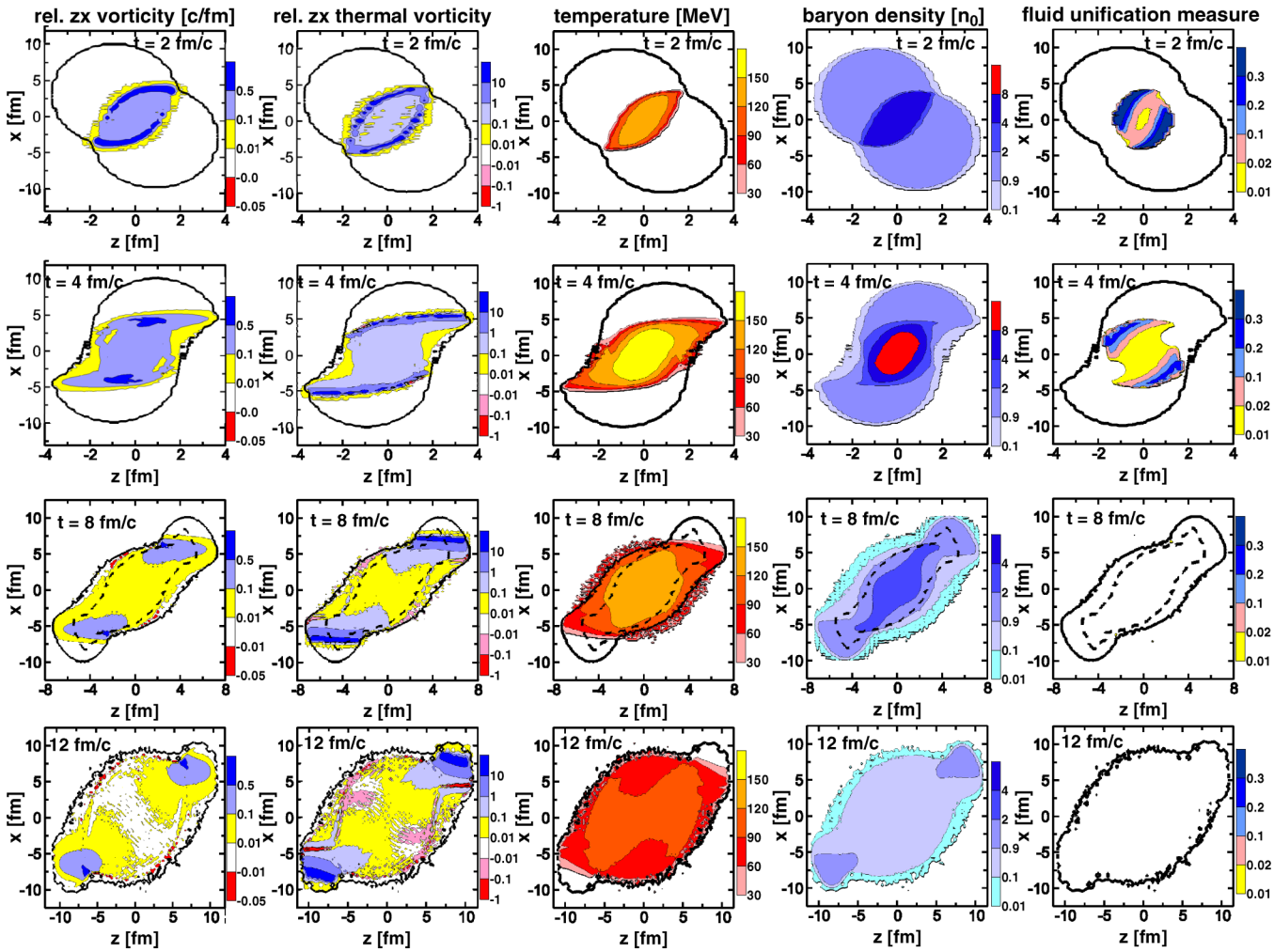

FIG. 2. Columns from left to right: The proper-energy-density weighted relativistic kinematic zx vorticity, the thermal zx vorticity, the temperature [cf. Eq. (8)], the proper baryon density (n_B) [cf. Eq. (6)] in units of the the normal nuclear density ($n_0 = 0.15\,1/\mathrm{fm}^3$), and the fluid unification measure [cf. Eq. (7)] of the baryon-rich subsystem, in the reaction plane at various time instants in the semicentral ($b = 6$ fm) Au+Au collision at $\sqrt{s_{NN}} = 4.9$ GeV. Calculations are done with the crossover EoS. The z axis is the beam direction. Note the different scale along the z axis at different time instants. The outer bold solid contour displays the border of the baryon-rich matter. Inside this contour $n_B/n_0 > 0.1$ at $t = 2, 4, 8$ fm/c and $n_B/n_0 > 0.01$ $t = 12$ fm/c.

Therefore, in order to keep all the matter in the consideration the freeze-out was turned off.

In order to suppress contributions of almost empty regions, where the matter is relatively thin, we consider a proper-energy-density-weighted relativistic kinematic vorticity in the reaction (xz) plane, i.e., at $y = 0$:

$$\Omega_{\mu\nu}(x,0,z,t) = \omega_{\mu\nu}(x,0,z,t)\varepsilon_B(x,0,z,t)/\langle\varepsilon_B(0,t)\rangle, \quad (9)$$

similar to that in Refs. [16,20]. Here

$$\langle\varepsilon_B(y,t)\rangle = \int dx\,dz\,\varepsilon_B(x,y,z,t) \Big/ \int_{\varepsilon_B(x,y,z,t)>0} dx\,dz \quad (10)$$

is the energy density of net-baryon-rich fluids, $\varepsilon_B = \varepsilon_p + \varepsilon_t$, averaged over an xz plane. Similarly to $\Omega_{\mu\nu}$, we define a proper-energy-density-weighted thermal vorticity in the reaction plane, though keeping the same notation ($\varpi_{\mu\nu}$) for it.

In Figs. 2 and 3, we present the proper-energy-density weighted relativistic kinematic zx vorticity [cf. Eqs. (9) and (10)] and the thermal zx vorticity, as well as the temperature and the proper baryon density, Eqs. (8) and (6), respectively, of the baryon-rich subsystem in the reaction plain (xz) at various time instants in semicentral ($b = 6$ fm) Au+Au collisions at $\sqrt{s_{NN}} = 4.9$ and 7.7 GeV. The figures also present the fluid unification measure [cf. Eq. (7)]. As already mentioned, the baryon-rich fluids are mutually stopped and unified at $t \gtrsim 4$ fm/c for 4.9 GeV and $t \gtrsim 2$ fm/c for 7.7 GeV. In particular, this means that the temperature and respectively the thermal vorticity are poorly defined at earlier time instants. When the freeze-out starts (the inner bold dashed contour in Figs. 2 and 3), the baryon-rich system has been already completely equilibrated. To the last displayed time instant ($t = 12$ fm/c) the freeze-out has been already completed.

In contrast to Refs. [20,21], where results averaged over all slices with different y coordinate were presented, we

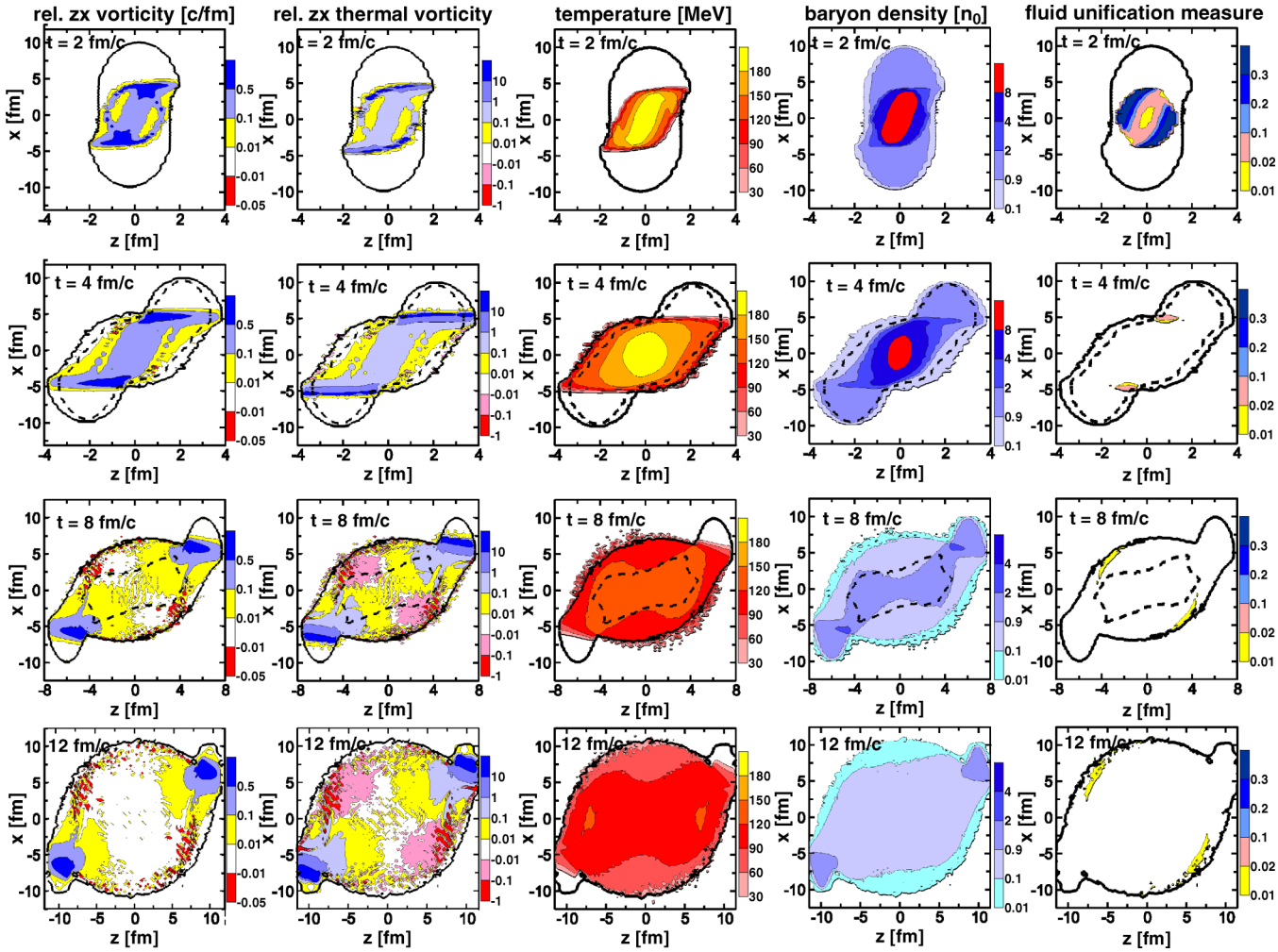

FIG. 3. The same as in Fig. 2 but at $\sqrt{s_{NN}} = 7.7$ GeV. At $t = 2$ fm/c there is no frozen-out matter, while at $t = 8$ fm/c all the matter is frozen out.

demonstrate plots of $\Omega_{\mu\nu}$ and $\varpi_{\mu\nu}$ for the single slice $y = 0$, i.e., the true reaction plane. It allows us to reveal certain qualitative features of the vorticity field.

As seen, the relativistic kinematic vorticity and thermal vorticity primarily start at the border between the participant and spectator matter. Later on they partially spread to the participant and spectator bulk, though remaining concentrated near the border. In the conventional hydrodynamics this extension into the bulk of the system is an effect of the shear viscosity. In the 3FD dynamics it is driven by the 3FD dissipation which imitates the effect of the shear viscosity [35]. The spread into the bulk is more spectacular at lower collision energy ($\sqrt{s_{NN}} = 4.9$ GeV) because of the higher effective shear viscosity than that at higher energies [35]. At the same time, the vorticity in the participant bulk gradually dissolves in the course of time and practically disappears in the center of the colliding system to the end of the collision.

This observation has consequences for the polarization of secondary produced particles. These particles are abundantly produced in the most dense and hot regions of the system, i.e., in the center of the colliding system. However, the vorticity is small there. The polarized particles dominantly originate from peripheral regions with high vorticity and quite moderate temperature; see right panels in Figs. 2 and 3. Therefore, we should not expect a large overall polarization of Λ hyperons in spite of high peak values of the vorticity. At the same time, the relative polarization of Λ hyperons should be higher in the fragmentation regions, i.e., the kinematical region of the participant-spectator border, than that in the midrapidity region. In the vorticity plots presented in Refs. [20,21] the vorticity occupies the bulk of the participants. This happens because of because of the averaging over all slices with different y coordinate applied there. This averaging smears out the vorticity peaks at the border.

As one can see, the peak values of the thermal vorticity reach extremely high values. This is because of strong gradients of the temperature at the border between the participant and spectator matter. These gradients enhance the thermal vorticity. The peak values cannot be directly compared with those presented in Refs. [20,21] because of the additional averaging over all slices with different y coordinate applied there. In order to perform a more informative comparison, we calculated relativistic (kinematic and thermal) zx vorticity of the baryon-rich subsystem in the semicentral ($b = 6$ fm)

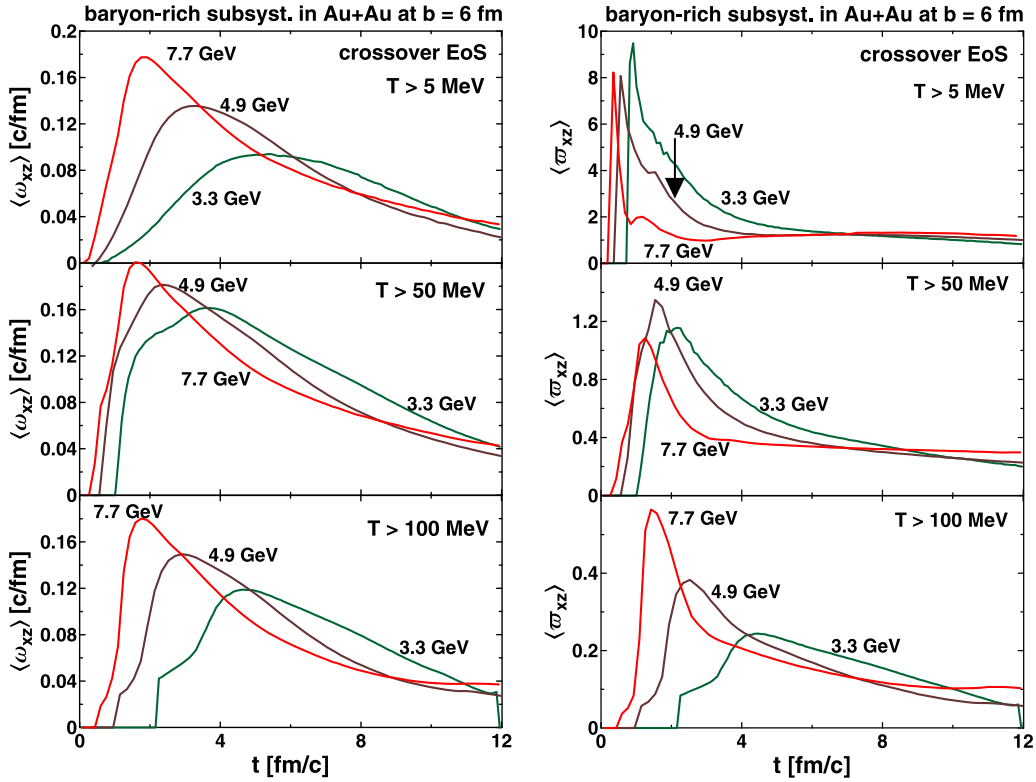

FIG. 4. Time evolution of relativistic kinematic zx vorticity (left column of panels) and thermal zx vorticity (right column of panels) of the baryon-rich subsystem in the semicentral ($b = 6$ fm) Au+Au collisions at $\sqrt{s_{NN}} = 3.3$, 4.9, and 7.7 GeV. The vorticities are averaged with the weight of the proper energy density over different regions with temperatures $T > 5$, 50, and 100 MeV.

Au+Au collision at $\sqrt{s_{NN}} = 3.3$, 4.9, and 7.7 GeV averaged with the weight of the proper energy density over the whole system; see Fig. 4. Keeping in mind that the Λ hyperons are abundantly produced from the hottest regions of the system, we applied certain constraints on this averaging. We considered three regions of the averaging: (i) a region with temperatures $T > 5$ MeV that in fact includes all the participant region, and two regions with more stringent constraints, i.e., (ii) $T > 50$ MeV and (iii) $T > 100$ MeV. These biased averaged quantities can be expressed as follows:

$$\langle \omega_{\mu\nu}(t)\rangle_{T>T_0} = \int_{T>T_0} dV\, \omega_{\mu\nu}(x,y,z,t)\, \varepsilon_B(x,y,z,t) \Big/ \int_{T>T_0} dV\, \varepsilon_B(x,y,z,t), \quad (11)$$

$$\langle \varpi_{\mu\nu}(t)\rangle_{T>T_0} = \int_{T>T_0} dV\, \varpi_{\mu\nu}(x,y,z,t)\, \varepsilon_B(x,y,z,t) \Big/ \int_{T>T_0} dV\, \varepsilon_B(x,y,z,t), \quad (12)$$

where T_0 is the temperature constraint.

Time evolution of the biased relativistic kinematic zx vorticity and thermal zx vorticity of the baryon-rich subsystem averaged with the weight of the proper energy density over the whole system is presented in Fig. 4. As seen, the kinematic vorticity weakly depends on the temperature constraint. At the initial (compression) stage of the collision the kinematic vorticity differs at different collision energies. However, at the expansion stage, i.e., after the maximum of $\langle \omega_{\mu\nu}(t)\rangle$, the kinematic vorticity becomes less sensitive to the collision energy. Moreover, the values of the kinematic vorticity are almost independent of the collision energy at the final ("freeze-out") stage, though this concerns quite a narrow range of collision energies. These final-stage values are compatible with those at $\sqrt{s_{NN}} = 5$ GeV obtained in Ref. [21] within the hadron-string dynamics model [22]. As compared with the results of Ref. [20] within the relativistic PICR hydro approach [16] at $\sqrt{s_{NN}} = 8$ GeV, the whole expansion PICR stage is very (quantitatively and qualitatively) similar to that in our simulations at $\sqrt{s_{NN}} = 7.7$ GeV.

It is worthwhile to mention that the averaged vorticity displayed in Fig. 4 does not coincide with that of the frozen-out system. The freeze-out in the 3FD model is a continuous-in-time process [23,34], as it is illustrated in Figs. 2 and 3. When the the freeze-out happens the frozen-out matter stops to hydrodynamically evolve. In particular, the achieved vorticity also turns out to be frozen out. In the calculation presented in Fig. 4 all the matter hydrodynamically evolves without exemptions till the very late time. Therefore, the late-stage values presented in Fig. 4 can be considered only as an estimate of the vorticity averaged over the frozen-out system.

Enormously high peak values of the thermal vorticity, see the right column of panels in Fig. 4, are irrelevant because of the above mentioned poor definition of this vorticity at the early stages of the collision, i.e., at $t \lesssim 4$ fm/c for 4.9 GeV and $t \lesssim 2$ fm/c for 7.7 GeV. The relativistic thermal zx vorticity

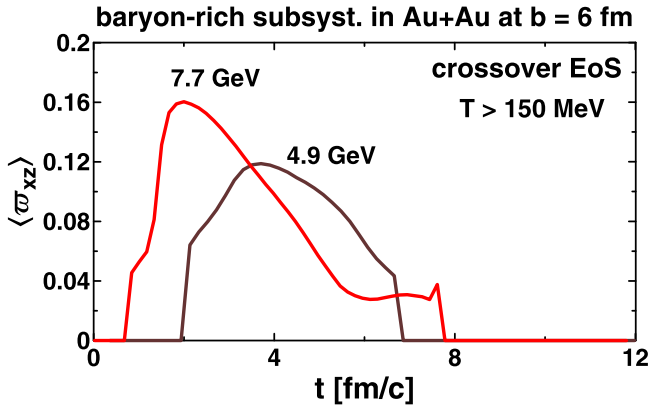

FIG. 5. The same as in Fig. 4 but for the relativistic thermal zx vorticity with the constraint $T > 150$ MeV.

averaged with the weight of the proper energy density over the whole system exhibits features similar to those observed in the relativistic kinematic zx vorticity except that $\langle\varpi_{\mu\nu}(t)\rangle$ strongly depends on the temperature constraint. This a consequence of the cutoff of near-spectator regions with high temperature gradients at the high-T_0 constraint; see Eq. (12). Nevertheless, even at the $T_0 = 100$ MeV cutoff the $\langle\varpi_{\mu\nu}(t)\rangle$ values at $\sqrt{s_{NN}} = 7.7$ GeV essentially exceed those reported in Ref. [20] for $\sqrt{s_{NN}} = 8$ GeV. This happens because the near-spectator regions still contribute even at the $T_0 = 100$ MeV cutoff. Only at $T_0 = 150$ MeV do our $\langle\varpi_{\mu\nu}(t)\rangle$ values become comparable with those of Ref. [20]; see Fig. 5. In view of the kinematic zx vorticity being well comparable within the present 3FD and PICR hydro [16] approaches, we can conclude that the temperature gradients in the periphery of the participant zone are much stronger in the 3FD model.

IV. SUMMARY

Within the 3FD model (crossover scenario) we have studied vorticity evolution in heavy-ion collisions at NICA energies. We considered two definitions of the vorticity—relativistic kinematic and thermal vorticities—that are relevant in different aspects of the rotation effects.

It is found that the vorticity mainly takes place at the border between participant and spectator matter. This effect was noticed in the analysis of the kinematic vorticity field [36,37] in the framework of the kinetic quark-gluon string model. The authors of Refs. [36,37] observed that the vorticity field is predominantly localized in a relatively thin layer on the boundary between participants and spectators and that it forms a specific toroidal structure—a so called femto-vortex sheet. As we found, this effect is essentially enhanced for the case of the thermal vorticity because of strong temperature gradients at the participant-spectator border. As the thermal vorticity is directly related to the Λ-hyperon polarization, this implies that the Λ-hyperon polarization should be stronger at peripheral rapidities, corresponding to the participant-spectator border, than that in the midrapidity region.

At the expansion stage of the collision the vorticity is only weakly dependent on the collision energy, though the considered NICA energy range is quite narrow. The order of magnitude of the mean weighted kinematic vorticity agrees with that estimated in Ref. [21] (for $\sqrt{s_{NN}} = 4.9$ GeV) and in Ref. [20] (for $\sqrt{s_{NN}} = 8$ GeV). At the same time, obtained values of the mean weighted thermal vorticity at $\sqrt{s_{NN}} = 7.7$ GeV, which is directly related to the Λ-hyperon polarization, are an order of magnitude higher than those reported in Ref. [20] for $\sqrt{s_{NN}} = 8$ GeV. An additional constraint to the high-temperature ($T > 150$ GeV) participant region, over which the mean values are calculated, reduces the mean values of the thermal vorticity by an order of magnitude and makes them comparable with those found in Ref. [20]. Only this strong constraint ($T > 150$ GeV) excludes the effect of strong temperature gradients at the participant-spectator border.

ACKNOWLEDGMENTS

Fruitful discussions with D.N. Voskresensky are gratefully acknowledged. We are also grateful to Oleg Teryaev for valuable comments on the manuscript of the paper. The calculations were performed at the computer cluster of GSI (Darmstadt). Y.B.I. was supported by the Russian Science Foundation, Grant No. 17-12-01427. A.A.S. was partially supported by the Ministry of Education and Science of the Russian Federation within the Academic Excellence Project of the NRNU MEPhI under Contract No. 02.A03.21.0005.

[1] F. Becattini, F. Piccinini, and J. Rizzo, Phys. Rev. C **77**, 024906 (2008).
[2] D. Kharzeev and A. Zhitnitsky, Nucl. Phys. A **797**, 67 (2007).
[3] O. V. Rogachevsky, A. S. Sorin, and O. V. Teryaev, Phys. Rev. C **82**, 054910 (2010).
[4] D. Kharzeev, Phys. Lett. B **633**, 260 (2006).
[5] K. Fukushima, D. E. Kharzeev, and H. J. Warringa, Phys. Rev. D **78**, 074033 (2008).
[6] A. R. Zhitnitsky, in *Strongly Interacting Matter in Magnetic Fields*, edited by D. Kharzeev, K. Landsteiner, A. Schmitt, and H.-U. Yee, Lecture Notes in Physics Vol. 871 (Springer, Berlin, 2013), p. 209.
[7] Z. T. Liang and X. N. Wang, Phys. Rev. Lett. **94**, 102301 (2005); **96**, 039901(E) (2006).
[8] B. Betz, M. Gyulassy, and G. Torrieri, Phys. Rev. C **76**, 044901 (2007).
[9] I. Karpenko and F. Becattini, Eur. Phys. J. C **77**, 213 (2017).
[10] Y. L. Xie, M. Bleicher, H. Stocker, D. J. Wang, and L. P. Csernai, Phys. Rev. C **94**, 054907 (2016).
[11] I. Upsal (STAR Collaboration), J. Phys. Conf. Ser. **736**, 012016 (2016); L. Adamczyk *et al.* (STAR Collaboration), arXiv:1701.06657.
[12] L. P. Csernai, D. D. Strottman, and C. Anderlik, Phys. Rev. C **85**, 054901 (2012).
[13] D. J. Wang, Z. Neda, and L. P. Csernai, Phys. Rev. C **87**, 024908 (2013).
[14] S. Floerchinger and U. A. Wiedemann, J. High Energy Phys. 11 (2011) 100; J. Phys. G **38**, 124171 (2011).

[15] X. G. Huang, P. Huovinen, and X. N. Wang, Phys. Rev. C **84**, 054910 (2011).
[16] L. P. Csernai, V. K. Magas, and D. J. Wang, Phys. Rev. C **87**, 034906 (2013).
[17] F. Becattini *et al.*, Eur. Phys. J. C **75**, 406 (2015).
[18] Y. Jiang, Z. W. Lin, and J. Liao, Phys. Rev. C **94**, 044910 (2016).
[19] W. T. Deng and X. G. Huang, Phys. Rev. C **93**, 064907 (2016).
[20] L. P. Csernai, D. J. Wang, M. Bleicher, and H. Stocker, Phys. Rev. C **90**, 021904 (2014).
[21] O. Teryaev and R. Usubov, Phys. Rev. C **92**, 014906 (2015).
[22] W. Cassing and E. L. Bratkovskaya, Phys. Rep. **308**, 65 (1999).
[23] Yu. B. Ivanov, V. N. Russkikh, and V. D. Toneev, Phys. Rev. C **73**, 044904 (2006).
[24] K. C. Meehan (STAR Collaboration), Nucl. Phys. A **956**, 878 (2016); J. Phys. Conf. Ser. **742**, 012022 (2016).
[25] Yu. B. Ivanov, Phys. Rev. C **87**, 064904 (2013).
[26] Y. B. Ivanov, Phys. Lett. B **721**, 123 (2013); Y. B. Ivanov and D. Blaschke, Phys. Rev. C **92**, 024916 (2015).
[27] Y. B. Ivanov, Phys. Rev. C **87**, 064905 (2013).
[28] Y. B. Ivanov, Phys. Rev. C **89**, 024903 (2014).
[29] Y. B. Ivanov and A. A. Soldatov, Phys. Rev. C **91**, 024914 (2015); Y. B. Ivanov, Phys. Lett. B **723**, 475 (2013).
[30] V. P. Konchakovski, W. Cassing, Y. B. Ivanov, and V. D. Toneev, Phys. Rev. C **90**, 014903 (2014); Y. B. Ivanov and A. A. Soldatov, *ibid.* **91**, 024915 (2015); Eur. Phys. J. A **52**, 10 (2016).
[31] F. Becattini, V. Chandra, L. Del Zanna, and E. Grossi, Ann. Phys. (N.Y.) **338**, 32 (2013).
[32] V. M. Galitsky and I. N. Mishustin, Sov. J. Nucl. Phys. **29**, 181 (1979).
[33] A. S. Khvorostukhin, V. V. Skokov, K. Redlich, and V. D. Toneev, Eur. Phys. J. C **48**, 531 (2006).
[34] V. N. Russkikh and Yu. B. Ivanov, Phys. Rev. C **76**, 054907 (2007); Yu. B. Ivanov and V. N. Russkikh, Phys. At. Nucl. **72**, 1238 (2009).
[35] Y. B. Ivanov and A. A. Soldatov, Eur. Phys. J. A **52**, 117 (2016); **52**, 367 (2016).
[36] M. I. Baznat, K. K. Gudima, A. S. Sorin, and O. V. Teryaev, Phys. Rev. C **93**, 031902 (2016).
[37] M. Baznat, K. Gudima, A. Sorin, and O. Teryaev, Phys. Rev. C **88**, 061901 (2013).